

# Direct Photoluminescence Probing of Ferromagnetism in Monolayer Two-Dimensional CrBr<sub>3</sub>

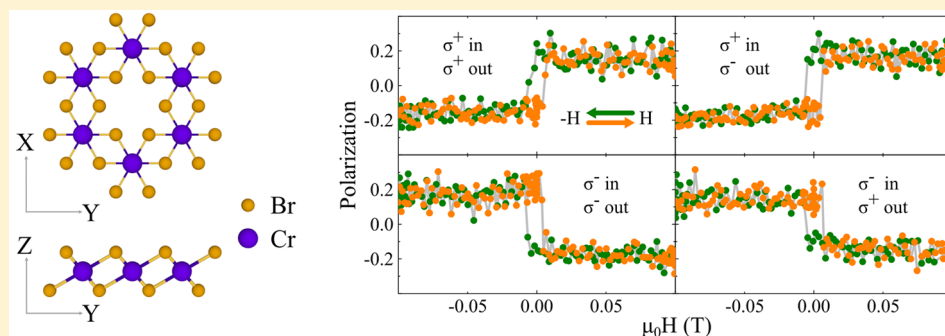
Zhaowei Zhang,<sup>†,||</sup> Jingzhi Shang,<sup>†,‡,||</sup> Chongyun Jiang,<sup>†,||</sup> Abdullah Rasmita,<sup>†</sup> Weibo Gao,<sup>\*,†,§</sup> and Ting Yu<sup>\*,†</sup>

<sup>†</sup>Division of Physics and Applied Physics, School of Physical and Mathematical Sciences, Nanyang Technological University, Singapore 637371, Singapore

<sup>‡</sup>Institute of Flexible Electronics, Northwestern Polytechnical University, 127 West Youyi Road, Xi'an 710072, China

<sup>§</sup>The Photonics Institute and Centre for Disruptive Photonic Technologies, Nanyang Technological University, Singapore 637371, Singapore

**S** Supporting Information



**ABSTRACT:** Atomically thin magnets are the key element to build up spintronics based on two-dimensional materials. The surface nature of two-dimensional ferromagnet opens up opportunities to improve the device performance efficiently. Here, we report the intrinsic ferromagnetism in atomically thin monolayer CrBr<sub>3</sub>, directly probed by polarization resolved magneto-photoluminescence. The spontaneous magnetization persists in monolayer CrBr<sub>3</sub> with a Curie temperature of 34 K. The development of magnons by the thermal excitation is in line with the spin-wave theory. We attribute the layer-number-dependent hysteresis loops in thick layers to the magnetic domain structures. As a stable monolayer material in air, CrBr<sub>3</sub> provides a convenient platform for fundamental physics and pushes the potential applications of the two-dimensional ferromagnetism.

**KEYWORDS:** Ferromagnetism, CrBr<sub>3</sub>, van der Waals, magnetic field

Ferromagnetism in atomically thin magnet has been studied in a variety of van der Waals materials,<sup>1,2</sup> including metallic Fe<sub>3</sub>GeTe<sub>2</sub>,<sup>3,4</sup> semiconducting Cr<sub>2</sub>Ge<sub>2</sub>Te<sub>6</sub><sup>5</sup> and insulating CrI<sub>3</sub>.<sup>6</sup> Even though the long-range magnetic order is highly suppressed by the thermal excitation of magnons in a two-dimensional (2D) magnet at finite temperature,<sup>7</sup> the magnetic anisotropy opens an energy gap in the magnon spectra and therefore protects the ferromagnetism in two dimensions. The magnon–magnon interaction in such van der Waals ferromagnets also provides a platform to study the fundamental topological spin excitation, for example, Dirac magnon<sup>8</sup> and topological magnon surface state.<sup>9</sup> Moreover, in contrast to the three-dimensional ferromagnet, magnetic 2D materials show tunable magnetic properties due to their surface nature.<sup>3,10–13</sup> In particular, the layer-number dependent<sup>4,6,14</sup> and gate-tunable magnetism<sup>3,10–13</sup> opens a new way to build spintronic devices with high accuracy and efficiency.<sup>15–20</sup>

Among various van der Waals ferromagnets, CrBr<sub>3</sub> is an interesting platform to study the magnetism in low dimensions

and light matter interactions in magnetic materials. The neutron scattering has revealed the Dirac points in bulk CrBr<sub>3</sub>,<sup>21,22</sup> formed by acoustic and optical spin-wave modes, where both intralayer and interlayer exchange interactions play an important role. On the other hand, optical absorption spectra in CrBr<sub>3</sub> have shown the out-of-plane magnetic field dependence,<sup>23</sup> suggesting potential applications in optoelectronics. However, magnetism in atomically thin CrBr<sub>3</sub>, especially in monolayer limit, is still unknown.

In this work, we demonstrate the ferromagnetism in 2D van der Waals CrBr<sub>3</sub>. We show the spontaneous magnetization in monolayer CrBr<sub>3</sub>, probed by d–d transition induced photoluminescence (PL) with a polarization-resolved optical confocal setup. The magnon excitation is limited at the low-

**Received:** February 7, 2019

**Revised:** March 25, 2019

**Published:** April 4, 2019

temperature region but shows an exponential development as further increasing the temperature, which is in line with the spin-wave theory. It is worthy to mention that  $\text{CrBr}_3$  is much more stable in air as compared to  $\text{CrI}_3$  as reported previously,<sup>6,24</sup> providing a convenient platform for magnetic material applications (Figure S1). Our study also shows the ferromagnetic interlayer coupling and magnetic domain-induced hysteresis loops in multilayers, providing an opportunity to use magnetic domains as the information carrier in a van der Waals magnet.

The atomic structure of monolayer  $\text{CrBr}_3$  is shown in Figure 1a.  $\text{Cr}^{3+}$  ions are arranged in a honeycomb lattice, and the

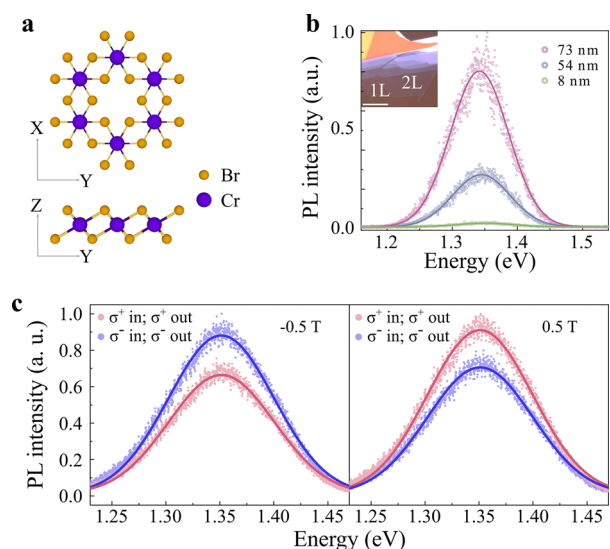


**Figure 1.** Crystal structure and PL of two-dimensional van der Waals  $\text{CrBr}_3$ . (a) Top view and side view of the atomic structure of monolayer  $\text{CrBr}_3$ . The  $\text{Cr}^{3+}$  ion was surrounded by six  $\text{Br}^-$  ions, forming an octahedral environment. The  $\text{Cr}-\text{Br}-\text{Cr}$  bond forms an angle of  $95.1^\circ$ . (b) PL spectra for  $\text{CrBr}_3$  with various thickness. Inset: Optical image of the exfoliated 2D  $\text{CrBr}_3$  on a quartz substrate. The scale bar is  $15 \mu\text{m}$ . (c) Polarization-resolved PL for monolayer  $\text{CrBr}_3$  at  $\pm 0.5 \text{ T}$ . All PL data were fitted by Gaussian functions.

$\text{Cr}-\text{Br}-\text{Cr}$  bond forms an angle of  $95.1^\circ$ , suggesting that ferromagnetic superexchange interaction is energetically favorable. To study the magnetism in two dimensions,  $\text{CrBr}_3$  flakes were exfoliated on a quartz substrate as shown in the inset of Figure 1b. Although in previous studies, reflection and absorption spectra have indicated the presence of  $^4\text{T}_2$  parity forbidden d–d transition<sup>23</sup> as shown in Figure S2, we first experimentally uncovered the d–d transition induced PL at  $1.35 \text{ eV}$  (Figure 1b), excited by a continuous wave (CW) laser at  $1.77 \text{ eV}$ . All measurements were performed at  $2.7 \text{ K}$ , unless otherwise specified. We studied the laser power dependent PL under the same polarization configuration (Figure S3). The PL intensity scales linearly with the laser power. This linear dependence rules out the possibility that the PL arises from the defect-bond excitons whose PL intensity trends to saturate while increasing the laser power.<sup>25</sup> We further examined the PL spectra for various layer-thicknesses as shown in Figure 1b. The PL peak energy almost does not change for the thickness ranging from  $6$  to  $73 \text{ nm}$ , which suggests a localized transition and is in agreement with the d–d transition as an interatom transition. According to Laporte rule, d–d transition is parity forbidden. To relax the Laporte rule, symmetry

breaking must be introduced, such as spin–orbit coupling, Jahn–Teller distortion, and the formation of odd-parity phonons.<sup>26</sup> The broad PL line width serves as the evidence for the strong vibronic coupling, resulting in phonon sidebands.

The d–d transition in the out-of-plane magnetic field shows circularly selective PL. Figure 1c shows the PL in  $-0.5$  and  $0.5 \text{ T}$  with  $\sigma^+\sigma^+$  and  $\sigma^-\sigma^-$  excitation–collection configurations, where  $\sigma^+$  ( $\sigma^-$ ) represents the left (right) circularly polarized light. The PL at  $\pm 0.5 \text{ T}$  shows opposite helicity, indicating that the spin of electrons in  $\text{CrBr}_3$  is coupled to the circularly polarized light.

The thickness of monolayer  $\text{CrBr}_3$  is around  $1 \text{ nm}$ , determined by atomic force microscope (AFM) (Figure S4). To precisely detect the magneto-PL in a single magnetic domain, the PL emission was collected by a single-mode optical fiber and detected by an avalanche photodiode (APD). Figure 2a shows the polarization as a function of the magnetic field under  $\sigma^+\sigma^+$ ,  $\sigma^-\sigma^-$ ,  $\sigma^+\sigma^-$ , and  $\sigma^-\sigma^+$  configurations. The polarization calculated by  $\rho = \frac{I_+ - I_-}{I_+ + I_-}$  is proportional to the magnetic moments, where  $I$  is the PL intensity recorded by APD while sweeping the magnetic field, and  $I_+$  ( $I_-$ ) is the PL intensity for the fully spin up (down) states (see Figure S5). Here, we set zero-polarization level where the PL intensity equals to  $(I_+ + I_-)/2$ . The green symbols show the evolution of the PL intensity with the magnetic field sweeping from  $0.1$  to  $-0.1 \text{ T}$ , and the orange symbols show the time reversal process.

We first discuss the polarization-resolved PL as a function of the magnetic field. There are three features in the Figure 2a: (i) the polarization abruptly increases or decreases within a narrow field range; (ii) except for the points near the transition field, the polarization is almost independent on the magnetic field; and (iii) the hysteresis loops have the same shape with the same excitation polarization, and it is independent to the polarization of the collection. We attribute these observations to the circularly selective absorption as shown in Figure 2b. Taking  $\sigma^+\sigma^+$  configuration as an example, at  $0.1 \text{ T}$  the electrons with up-spin selectively absorb the  $\sigma^+$  light and are excited to the upper states. As the magnetic field is swept to a negatively large point, thereby flipping the spin, less electrons can be excited by the  $\sigma^+$  light. Therefore, the polarization suddenly drops. In the time reversal process, the polarization shows a rapid increase at a certain field. The collection–polarization independent hysteresis loop is assigned to the depolarization of electrons at the excited state due to the electron–phonon scattering. This is consistent with the strong vibronic coupling in the d–d transition. This electric dipole transition provides a way to optically probe the magnetic state of the 2D  $\text{CrBr}_3$ .<sup>26</sup>

The nonzero polarization at zero magnetic field ( $0 \text{ T}$ ) indicates the presence of spontaneous magnetization in monolayer  $\text{CrBr}_3$ . To further confirm the intrinsic ferromagnetism, we measured the hysteresis loops with various laser powers ranging from  $10$  to  $100 \mu\text{W}$  (Figure S6). Even though the APD count increases with the excitation power, the polarization as a function of the magnetic field does not change much. The laser power independent hysteresis loops rule out the effect of thermal excitation on the magnetization. We also studied the magneto-optical Kerr effect (MOKE) in the monolayer  $\text{CrBr}_3$  on the  $\text{Si}/\text{SiO}_2$  substrate as shown in Figure S7a, which agrees with magnetic hysteresis loops probed by PL.

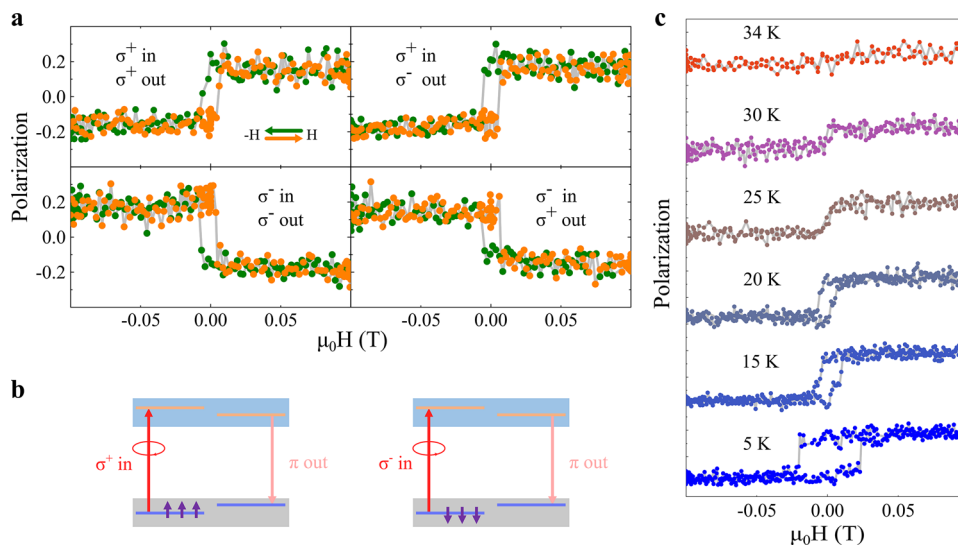


**Figure 2.** Ferromagnetism in monolayer  $\text{CrBr}_3$ . (a) Polarization as a function of the magnetic field. The orange symbols show the polarization as the magnetic field is swept from  $-0.1$  to  $0.1$  T and the green symbols show the polarization as the magnetic field is swept from  $0.1$  T to  $-0.1$  T. The none-zero polarization at zero magnetic field indicates the spontaneous magnetization.  $\sigma^+$  ( $\sigma^-$ ) is the left (right) circularly polarized light. (b) Origin of the magnetic field dependent PL. The helicity of the absorption ties to the spin of the electrons at the ground states. The unbalance of the spin-up and spin-down states makes a higher  $\sigma^+$ / $\sigma^-$  absorption and eventually leads to the high/low PL emission. Because of the phonon scattering at the excited state, the output light is depolarized ( $\pi$ ). (c) Hysteresis loops at various temperatures. The hysteresis loop disappears as the temperature was increased above the Curie temperature  $T_C$  at 34 K, slightly lower than that of the bulk crystal.

The ferromagnetism in monolayer results from the Cr—Br—Cr superexchange interaction. In monolayer  $\text{CrBr}_3$ , six  $\text{Cr}^{3+}$  ions form a honeycomb structure and each  $\text{Cr}^{3+}$  ion is surrounded by six  $\text{Br}^-$ , forming an octahedral environment (Figure 1a). In this crystal field, the degeneracy of d orbit of Cr atom is lifted and the d level splits into  $t_{2g}$  and  $e_g$  bands. Three spin polarized electrons occupy the  $t_{2g}$  band according to Hund's first rule. Therefore, the magnetic moment of each  $\text{Cr}^{3+}$  ion yields is  $\sim 3 \mu_B$ , corresponding to the polarization of 0.175 in monolayer case. The magnetic moments of monolayer  $\text{CrBr}_3$  align in the out-of-plane direction. The XXZ spin Hamiltonian<sup>27</sup> is adopted to describe the 2D ferromagnet:  $H_{\text{spin}} = -A \sum_i (S_i^z)^2 - J \sum_{i,j} S_i^z S_j^z - \lambda \sum_{i,j} S_i^z S_j^z$  where  $A$  is the single-ion anisotropy term,  $J$  is the Heisenberg exchange term, and  $\lambda$  is the anisotropic exchange term. The quenched d-orbit results in a negligible single-ion anisotropy term and thereby  $A$  is almost zero. The angle of the Cr—Br—Cr bond is around  $90^\circ$ , which favors a ferromagnetic intralayer coupling and  $J > 0$ . The out-of-plane magnetic anisotropy corresponds to  $\lambda > 0$ .

The Curie temperature was experimentally determined by measuring the hysteresis loops at various temperatures (Figure 2c). When the temperature was increased above the Curie temperature at 34 K, a ferromagnetism-to-paramagnetism phase transition occurred. The  $T_C$  of 34 K is only slightly lower than that of the bulk (i.e., 37 K). Figure 3 shows the polarization as a function of the temperature. The excitation of magnon by thermal fluctuation degrades the long-range magnetic order. We describe the reduced polarization as increasing the temperature within a spin-wave theory.<sup>27</sup> In an isotropic 2D spin system, the gapless magnon spectra leads to the absence of the spontaneous magnetization at finite temperature. Nevertheless,  $\Delta_0$ , the spin wave gap, opens by the anisotropic energy and protects the long-range magnetic order, which plays an essential role in the 2D ferromagnet. The magnetization in units of  $\hbar$  per Cr atom as a function of the temperature is described as  $M(T) = S - \frac{k_B T}{2\pi J S} e^{-\Delta_0/k_B T}$ , where

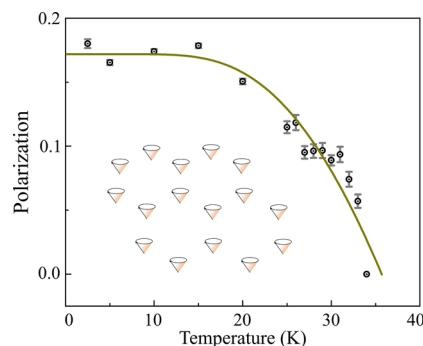


**Figure 3.** The polarization as a function of temperature for monolayer  $\text{CrBr}_3$ . The data is fitted by  $\rho(T) \sim S - \frac{k_B T}{2\pi J S} e^{-\Delta_0/k_B T}$ . Spin wave is excited by the thermal fluctuation, which causes the decay of the polarization as increasing the temperature.

$S = 3/2$ , and  $k_B$  is Boltzmann constant.<sup>27</sup> The polarization  $\rho$  is proportional to the  $M$ :  $\rho(T) \sim S - \frac{k_B T}{2\pi J S} e^{-\Delta_0/k_B T}$ . The solid line in Figure 3 shows the fitting results with this model in line with our experimental data. In the low temperature region ( $< 15$  K), the polarization weakly depends on the temperature. Further increasing the temperature leads to an exponential development of magnons and the polarization rapidly decreases until vanishing at the  $T_C$ .

Next, we study the layer—layer interaction in 2D van der Waals  $\text{CrBr}_3$ . The interlayer coupling is revealed by a bilayer  $\text{CrBr}_3$  with the thickness of about 2 nm, determined by AFM (Figure S4). Distinct from bilayer  $\text{CrI}_3$ , whose interlayer coupling at the ground states was antiferromagnetic,<sup>6</sup> bilayer  $\text{CrBr}_3$  preserves ferromagnetism as shown in Figure 4a, suggesting a ferromagnetic interlayer coupling. Note that the transition field for bilayer  $\text{CrBr}_3$  from fully spin up states to fully spin down states is almost one order smaller than that for



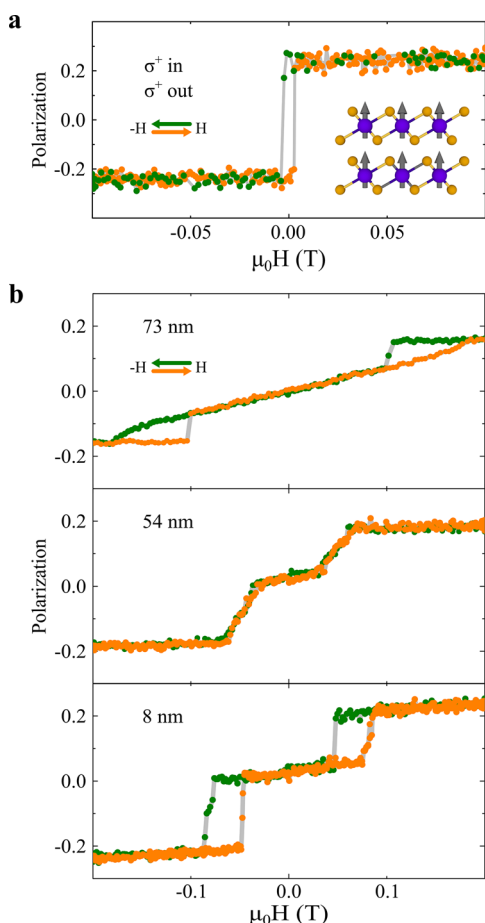


**Figure 4.** Layer-dependent magnetism in CrBr<sub>3</sub>. (a) The hysteresis loop for bilayer CrBr<sub>3</sub>. A nonzero polarization at zero magnetic field indicates a ferromagnetic interlayer coupling. (b) The polarization as a function of the magnetic field for 8, 54, and 73 nm CrBr<sub>3</sub>. The formation of the strip- or honeycomb-like magnetic domains may account for the layer-dependent magnetism in CrBr<sub>3</sub>.

bilayer CrI<sub>3</sub>.<sup>6</sup> This is in line with the different anisotropic energies of these two ferromagnetic insulators.

Finally, we discuss the magnetism in multilayer CrBr<sub>3</sub>. Figure 4b shows the polarization as a function of the magnetic field for 8, 54, and 73 nm samples. Different from the thin sample, whose rectangular hysteresis loops indicate single-domain and fully out-of-plane anisotropic magnetic ordering, the polarization of thicker CrBr<sub>3</sub> samples vanishes at 0 T. As the magnetic field was increased, the polarization became saturated after reaching a transition field, being similar to that of previously reported multilayer Fe<sub>3</sub>GeTe<sub>2</sub><sup>4</sup> and Co/Pt thin films.<sup>28</sup> We attribute this magnetic behavior to the formation of strip- and honeycomb-like magnetic domain structures as reported in ref 29 which is beyond the resolution of the PL setup. The spot size of our excitation laser is about 1  $\mu\text{m}$ , and thereby the polarization is contributed by several domains. As a result, the polarization at 0 T vanishes and shows a gradual evolution as increasing the magnetic field and abruptly saturates at a certain magnetic field. The possible reason for forming these kinds of domains might be the low out-of-plane anisotropic energy in thick CrBr<sub>3</sub>.<sup>30</sup> Even in a very low temperature (2.5 K), the ratio of out-of-plane anisotropy to the exchange interaction is strongly dependent on the dimension. The enhanced out-of-plane anisotropy in thin layers might

result from a reduced screening effect.<sup>24</sup> Even though we could expect a higher  $T_C$  with a larger out-of-plane anisotropy, the competition of the increased thermal fluctuation in thin layers eventually makes the  $T_C$  slightly lower than that of bulk.

To conclude, we demonstrate ferromagnetism in atomically thin CrBr<sub>3</sub> through polarization resolved magneto-PL. In monolayer CrBr<sub>3</sub>, a rectangular hysteresis loop shows that the spontaneous magnetization persists despite the thermal fluctuation. The polarization vanishes at 34 K due to the excitation of magnons. We also reveal the ferromagnetic interlayer coupling in a bilayer. Finally, the hysteresis loops of thick layers are assigned to the formation of strip- and honeycomb-like magnetic domains, whose magnetization is strongly dependent on the layer number of CrBr<sub>3</sub>. Our study uncovers the magnetism in 2D CrBr<sub>3</sub> and might pave a way for novel optoelectronic and spintronic devices.

**Methods.** We fabricated atomically thin CrBr<sub>3</sub> layers by mechanical exfoliation on a quartz substrate in an argon-filled glovebox. The thickness of the sample was first estimated by optical contrast and then confirmed by AFM. After fabrication, the sample was loaded into a magneto-cryostat (Cryomag-netics close-cycle cryostat) with an out-of-plane magnetic field ranging from  $-7$  to  $7$  T. We used a homemade fiber-based confocal microscope to perform the polarization-resolved PL. Polarizers and waveplates were equipped on the excitation and collection arms to selectively excite and detect circularly polarized light. The PL spectra were obtained by a spectrometer (Andor Shamrock) with a CCD detector. To measure the hysteresis loops, the PL emission was collected by a single-mode fiber and detected by an APD.

## ■ ASSOCIATED CONTENT

### 📄 Supporting Information

The Supporting Information is available free of charge on the ACS Publications website at DOI: 10.1021/acs.nanolett.9b00553.

Additional details on configurational coordinate diagram for the  $^4A_2$  to  $^4T_2$  d–d transition, PL intensity as a function of the excitation laser power with a linear fitting, AFM images for monolayer and bilayer CrBr<sub>3</sub>, the definition of the polarization, hysteresis loops at various excitation laser powers, MOKE for two-dimensional CrBr<sub>3</sub>, and temperature-dependent hysteresis loops for bilayer and 73 nm CrBr<sub>3</sub> (PDF)

## ■ AUTHOR INFORMATION

### Corresponding Authors

\*E-mail: wbgao@ntu.edu.sg.

\*E-mail: yuting@ntu.edu.sg.

### ORCID

Jingzhi Shang: 0000-0002-7451-777X

Weibo Gao: 0000-0003-3971-621X

### Author Contributions

||Z.Z., J.S., and C.J. contributed equally.

### Notes

The authors declare no competing financial interest.

## ■ ACKNOWLEDGMENTS

We acknowledge the support from the Singapore National Research Foundation through a Singapore 2015 NRF fellowship grant (NRF-NRFF2015-03) and its Competitive

Research Program (CRP Award No. NRF-CRP14-2014-02), Singapore Ministry of Education (MOE2017-T1-RG19/17, MOE2017-T1-RG199/17, MOE2018-T2-2-072, MOE2016-T2-2-077 and MOE2016-T2-1-163), A\*Star QTE programme, a start-up Grant (M4081441) from Nanyang Technological University and the Fundamental Research Funds for the Central Universities of China.

## REFERENCES

- (1) Burch, K. S.; Mandrus, D.; Park, J. G. Magnetism in two-dimensional van der Waals materials. *Nature* **2018**, *563*, 47–52.
- (2) Gong, C.; Zhang, X. Two-dimensional magnetic crystals and emergent heterostructure devices. *Science* **2019**, *363*, eaav4450.
- (3) Deng, Y.; Yu, Y.; Song, Y.; Zhang, J.; Wang, N. Z.; Sun, Z.; Yi, Y.; Wu, Y. Z.; Wu, S.; Zhu, J.; Wang, J.; Chen, X. H.; Zhang, Y. Gate-tunable room-temperature ferromagnetism in two-dimensional  $\text{Fe}_3\text{GeTe}_2$ . *Nature* **2018**, *563*, 94–99.
- (4) Fei, Z.; Huang, B.; Malinowski, P.; Wang, W.; Song, T.; Sanchez, J.; Yao, W.; Xiao, D.; Zhu, X.; May, A. F.; Wu, W.; Cobden, D. H.; Chu, J. H.; Xu, X. Two-dimensional itinerant ferromagnetism in atomically thin  $\text{Fe}_3\text{GeTe}_2$ . *Nat. Mater.* **2018**, *17*, 778–782.
- (5) Gong, C.; Li, L.; Li, Z.; Ji, H.; Stern, A.; Xia, Y.; Cao, T.; Bao, W.; Wang, C.; Wang, Y.; Qiu, Z. Q.; Cava, R. J.; Louie, S. G.; Xia, J.; Zhang, X. Discovery of intrinsic ferromagnetism in two-dimensional van der Waals crystals. *Nature* **2017**, *546*, 265–269.
- (6) Huang, B.; Clark, G.; Navarro-Moratalla, E.; Klein, D. R.; Cheng, R.; Seyler, K. L.; Zhong, D.; Schmidgall, E.; McGuire, M. A.; Cobden, D. H.; Yao, W.; Xiao, D.; Jarillo-Herrero, P.; Xu, X. D. Layer-dependent ferromagnetism in a van der Waals crystal down to the monolayer limit. *Nature* **2017**, *546*, 270–273.
- (7) Mermin, N. D.; Wagner, H. Absence of Ferromagnetism or Antiferromagnetism in One- or Two-Dimensional Isotropic Heisenberg Models. *Phys. Rev. Lett.* **1966**, *17*, 1133–1136.
- (8) Pershobuba, S. S.; Banerjee, S.; Lashley, J. C.; Park, J.; Ågren, H.; Aeppli, G.; Balatsky, A. V. Dirac Magnons in Honeycomb Ferromagnets. *Phys. Rev. X* **2018**, *8*, 011010.
- (9) Chen, L.; Chung, J.-H.; Gao, B.; Chen, T.; Stone, M. B.; Kolesnikov, A. I.; Huang, Q.; Dai, P. Topological Spin Excitations in Honeycomb Ferromagnet  $\text{CrI}_3$ . *Phys. Rev. X* **2018**, *8*, 041028.
- (10) Huang, B.; Clark, G.; Klein, D. R.; MacNeill, D.; Navarro-Moratalla, E.; Seyler, K. L.; Wilson, N.; McGuire, M. A.; Cobden, D. H.; Xiao, D.; Yao, W.; Jarillo-Herrero, P.; Xu, X. Electrical control of 2D magnetism in bilayer  $\text{CrI}_3$ . *Nat. Nanotechnol.* **2018**, *13*, 544–548.
- (11) Jiang, S.; Li, L.; Wang, Z.; Mak, K. F.; Shan, J. Controlling magnetism in 2D  $\text{CrI}_3$  by electrostatic doping. *Nat. Nanotechnol.* **2018**, *13*, 549–553.
- (12) Jiang, S.; Shan, J.; Mak, K. F. Electric-field switching of two-dimensional van der Waals magnets. *Nat. Mater.* **2018**, *17*, 406–410.
- (13) Wang, Z.; Zhang, T.; Ding, M.; Dong, B.; Li, Y.; Chen, M.; Li, X.; Huang, J.; Wang, H.; Zhao, X.; Li, Y.; Li, D.; Jia, C.; Sun, L.; Guo, H.; Ye, Y.; Sun, D.; Chen, Y.; Yang, T.; Zhang, J.; Ono, S.; Han, Z.; Zhang, Z. Electric-field control of magnetism in a few-layered van der Waals ferromagnetic semiconductor. *Nat. Nanotechnol.* **2018**, *13*, 554–559.
- (14) Bonilla, M.; Kolekar, S.; Ma, Y.; Diaz, H. C.; Kalappattil, V.; Das, R.; Eggers, T.; Gutierrez, H. R.; Phan, M. H.; Batzill, M. Strong room-temperature ferromagnetism in  $\text{VSe}_2$  monolayers on van der Waals substrates. *Nat. Nanotechnol.* **2018**, *13*, 289–293.
- (15) Jiang, S.; Li, L.; Wang, Z.; Shan, J.; Mak, K. F. Spin transistor build on 2D van der Waals heterostructures. *Nat. Nanotechnol.* **2018**, *13*, 549.
- (16) Klein, D. R.; MacNeill, D.; Lado, J. L.; Soriano, D.; Navarro-Moratalla, E.; Watanabe, K.; Taniguchi, T.; Manni, S.; Canfield, P.; Fernández-Rossier, J.; et al. Probing magnetism in 2D van der Waals crystalline insulators via electron tunneling. *Science* **2018**, *360*, 1218–1222.
- (17) Song, T.; Cai, X.; Tu, M. W.-Y.; Zhang, X.; Huang, B.; Wilson, N. P.; Seyler, K. L.; Zhu, L.; Taniguchi, T.; Watanabe, K.; et al. Giant tunneling magnetoresistance in spin-filter van der Waals heterostructures. *Science* **2018**, *360*, 1214–1218.
- (18) Song, T.; Tu, M. W.-Y.; Carnahan, C.; Cai, X.; Taniguchi, T.; Watanabe, K.; McGuire, M. A.; Cobden, D. H.; Xiao, D.; Yao, W.; et al. Voltage Control of a van der Waals Spin-Filter Magnetic Tunnel Junction. *Nano Lett.* **2019**, *19*, 915–920.
- (19) Kim, H. H.; Yang, B.; Patel, T.; Sfigakis, F.; Li, C.; Tian, S.; Lei, H.; Tsen, A. W. One Million Percent Tunnel Magnetoresistance in a Magnetic van der Waals Heterostructure. *Nano Lett.* **2018**, *18*, 4885–4890.
- (20) Wang, Z.; Gutierrez-Lezama, I.; Ubrig, N.; Kroner, M.; Gibertini, M.; Taniguchi, T.; Watanabe, K.; Imamoglu, A.; Giannini, E.; Morpurgo, A. F. Very large tunneling magnetoresistance in layered magnetic semiconductor  $\text{CrI}_3$ . *Nat. Commun.* **2018**, *9*, 2516.
- (21) Samuelsen, E. J.; Silbergliitt, R.; Shirane, G.; Remeika, J. P. Spin Waves in Ferromagnetic  $\text{CrBr}_3$  Studied by Inelastic Neutron Scattering. *Phys. Rev. B* **1971**, *3*, 157–166.
- (22) Yelon, W. B.; Silbergliitt, R. Renormalization of Large-Wave-Vector Magnons in Ferromagnetic  $\text{CrBr}_3$  Studied by Inelastic Neutron Scattering: Spin-Wave Correlation Effects. *Phys. Rev. B* **1971**, *4*, 2280–2286.
- (23) Dillon, J. F. J.; Kamimura, H.; Remeika, J. P. Magneto-optical properties of ferromagnetic chromium trihalides. *J. Phys. Chem. Solids* **1966**, *27*, 1531–1549.
- (24) Jin, W.; Kim, H. H.; Ye, Z.; Li, S.; Rezaie, P.; Diaz, F.; Siddiq, S.; Wauer, E.; Yang, B.; Li, C.; Tian, S.; Sun, K.; Lei, H.; Tsen, A. W.; Zhao, L.; He, R. Raman fingerprint of two terahertz spin wave branches in a two-dimensional honeycomb Ising ferromagnet. *Nat. Commun.* **2018**, *9*, 5122.
- (25) Tongay, S.; Suh, J.; Ataca, C.; Fan, W.; Luce, A.; Kang, J. S.; Liu, J.; Ko, C.; Raghunathan, R.; Zhou, J.; Ogletree, F.; Li, J. B.; Grossman, J. C.; Wu, J. Q. Defects activated photoluminescence in two-dimensional semiconductors: interplay between bound, charged, and free excitons. *Sci. Rep.* **2013**, *3*, 2657.
- (26) Seyler, K. L.; Zhong, D.; Klein, D. R.; Gao, S. Y.; Zhang, X. O.; Huang, B.; Navarro-Moratalla, E.; Yang, L.; Cobden, D. H.; McGuire, M. A.; Yao, W.; Xiao, D.; Jarillo-Herrero, P.; Xu, X. D. Ligand-field helical luminescence in a 2D ferromagnetic insulator. *Nat. Phys.* **2018**, *14*, 277–281.
- (27) Lado, J. L.; Fernández-Rossier, J. On the origin of magnetic anisotropy in two dimensional  $\text{CrI}_3$ . *2D Mater.* **2017**, *4*, 035002.
- (28) Pierce, M. S.; Buechler, C. R.; Sorensen, L. B.; Turner, J. J.; Kevan, S. D.; Jagla, E. A.; Deutsch, J. M.; Mai, T.; Narayan, O.; Davies, J. E.; Liu, K.; Dunn, J. H.; Chesnel, K. M.; Kortright, J. B.; Hellwig, O.; Fullerton, E. E. Disorder-induced microscopic magnetic memory. *Phys. Rev. Lett.* **2005**, *94*, 017202.
- (29) Kuhlrow, B.; Lambeck, M. Magnetic domain structures in  $\text{CrBr}_3$ . *Physica B+C* **1975**, *80*, 365–373.
- (30) Jagla, E. A. Hysteresis loops of magnetic thin films with perpendicular anisotropy. *Phys. Rev. B: Condens. Matter Mater. Phys.* **2005**, *72*, 094406.